

**Numerical Study on Micropolar Nanofluid Flow over an Inclined Surface by Means of Keller-Box**

**Abstract**

In this paper, Micropolar Nanofluid boundary layer flow over linear inclined extending surface with magnetic effect investigated. Model utilized in this examination depends on Buongiorno model for the thermal efficiencies of the liquid flow in the presence of Brownian movements and thermophoresis properties. The nonlinear problem for Micropolar Nanofluid flow over slanted channel is demonstrated to consider the heat and mass exchange marvel by considering portent flow parameters to strengthened boundary layers. The administering nonlinear partial differential equations are changed to nonlinear ordinary equations and a short time later outlined numerically by strategies for the Keller-Box plan. A correlation of the set up results in the absence of the incorporated impacts is performed with the accessible results and perceived in a decent settlement. Numerical and graphical outcomes are additionally exhibited in tables and diagrams.

**Keywords:** Micropolar Nanofluid, MHD, inclined surface.

**1 Introduction**

Nanofluids set up a subclass of sub-atomic liquids intended to work at the nanoscale. Nanofluids comprise connection between mass materials and sub-atomic structure. The quick advancement of nanotechnology has seen a critical consideration in such fluids through the entire expansiveness of assembling, including building, aviation, restorative creations and vitality innovations. Nanofluid is a blend of various nanoparticles, for example, aluminum, silver, copper and titanium with or without their oxides and base liquids including water, ethylene glycol and oil and so forth when nanoparticles deliberately scattered in the base liquids, the subsequent nanofluids have been affirmed to achieve critical enhancement in the properties of thermal conductivity, introduced by Choi [1]. The elements that play essential principle to upgrade the thermal conductivity of nanofluid has been considered by Buongiorno [2]. He found that the thermal conductivity of the fluid increment due to thermophoresis and Brownian movement impacts in the ordinary liquid. Brownian movement is the unpredictable development of the nanoparticles in the conventional liquid and caused the constant impacts between based liquid and nanoparticles. Thermophoresis is the wonder which diffuses the particles because of the temperature inclination. The heat transfer of nanofluid over a nonlinear porous

sheet is numerically discussed by Zaimi et al. [3]. Anwar et al. [4] contemplated the numerical investigation of micropolar nanofluid flow over an extending sheet. Nanofluid flow over a slanted extending surface concentrated by Sandeep and Kumar [5]. They researched heat and mass exchange of dusty nanoparticles improved on account of the volume division of nano particles. Suriyakumar and Devi [6] communicated the impacts of inner heat generation and suction on blended convective nanofluid flow through slanted surface. Ziaei-Rad et al. [7] examined the similarity solution of boundary layer nanofluid flow on an inclined surface. Rashad [8] studied nanofluid flow by considering convective boundaries and anisotropic slip effect. Mitra [9] investigated computational modeling of nanofluid flow over a heated inclined plate. Khan et al. [10] outlined the heat and mass exchange of MHD Jeffery nanofluid flow over slanted sheet. Hatami et al. [11] examined three dimensional relentless nanofluid over a slanted plate.

The boundary layer flow over a slanted extending surface turn into an intriguing field of research on account of its uses in building, for example, paper creation, skin rubbing, grain stockpiling and drag generation. The investigation of boundary layer flow over ceaseless surface begun by Sakiadis [12]. Also, Crane [13] examined the closed form arrangement of boundary layer flow over an extending sheet. The boundary layer stream of dusty liquid over a slanted surface with heat source/sink introduced by Ramesh et al. [14]. Singh [15] explored heat and mass exchange of thick liquid on porous slanted plate. Similarity solution of magnetohydrodynamic flow over a slanted sheet examined by Ali et al. [16]. Ramesh et al. [17] took a shot at the boundary layer flow over slanted sheet with convective limits. MHD free convection dissipative liquid flow past over a slanted permeable surface was examined by Malik [18]. Hayat et al. [19] investigated radiation effect on the flow induced by stretching cylinder by considering non-uniform heat source/sink. Balla et al. [20] examined an inclined porous cavity filled with nanofluid saturated in permeable medium.

Micropolar liquids are those, which contain unbending arbitrarily situated particles submerged in a gooey medium with microstructure constituent, where bending of the molecule is unnoticed. Eringen [21] built up another reasoning of micropolar liquid to check the impact of small scale revolutions on smooth movement. Rahman et al. [22] talked about the flow of micropolar liquid by thinking about the variable properties. Micropolar fluid flow by taking different effects over an inclined sheet studied by Das [23]. Kasim et al. [24] inspected the micropolar liquid flow on the slanted plate numerically. Srinivasacharya and Bindu [25] researched micropolar liquid move through a slanted channel having parallel plates. Hazbavi and Sharhani [26] analyzed the flow of micropolar liquid between two parallel plates with steady weight slope. Shamshuddin et al. [27] contemplated the heat and mass exchange of micropolar liquid flow through penetrable slanted plate. The impact of two fold scattering on micropolar liquid flow over a slanted surface examined by Srinivasacharya et al. [28].

## **2 Problem formulation**

A steady, two dimensional boundary layer flow of micropolar Nano fluid over a permeable inclined linear stretching plate with an angle  $\gamma$  is considered. The stretching and free stream velocities are supposed to be as,  $u_w(x) = ax$  and  $u_\infty(x) = 0$  respectively, here ' $x$ ' is the coordinate dignified lengthways the enlarging surface and ' $a$ ' is a constant. An external transverse magnetic field is taken normal to the flow path. It is supposed that the electric and magnetic field effects are very minor as the magnetic Reynolds number is less Mishra et al. [29]. The micropolar finite size particles along with Nano particles are constantly distributed in the base fluids. The fluid particles have extra space to travel about formerly hitting to the other fluid particle, where these particles revolve in the fluid field and fallouts for spinning effects in the micropolar nanofluid. The Brownian motion and thermophoresis effects are taken into account. The temperature  $T$  and Nano particle fraction  $C$  at the wall take the constant values  $T_w$  and  $C_w$ , while the ambient forms used for nanofluid temperature and mass fractions  $T_\infty$  and  $C_\infty$  are attained as  $y$  lean towards to immensity shown in fig.1.

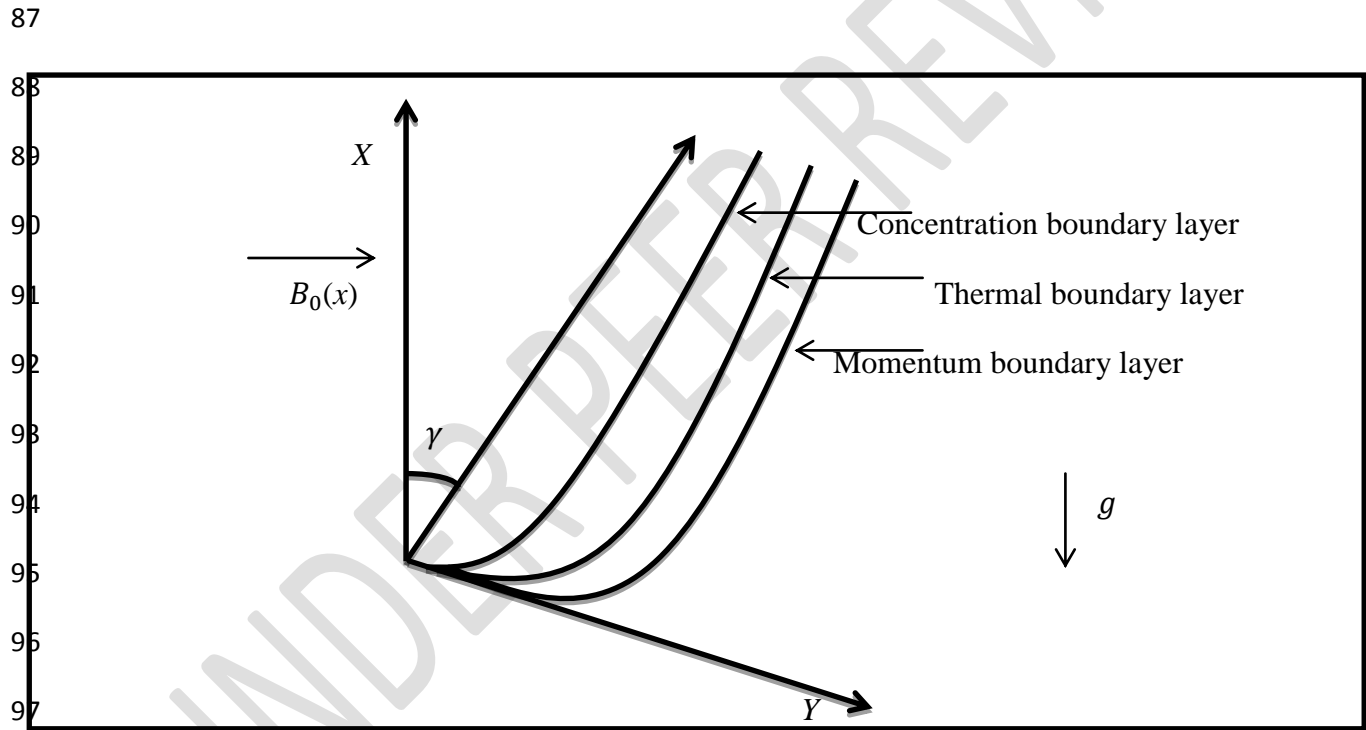


**Fig.1.** Physical geometry and coordinate system

The flow equations for this study are given by

$$\frac{\partial u}{\partial x} + \frac{\partial v}{\partial y} = 0, \quad (1)$$

$$u \frac{\partial u}{\partial x} + v \frac{\partial u}{\partial y} = \left( \frac{\mu + K_1^*}{\delta} \right) \frac{\partial^2 u}{\partial y^2} + \left( \frac{K_1^*}{\rho} \right) \frac{\partial N^*}{\partial y} + g[\beta_t(T - T_\infty) - \beta_c(C - C_\infty)] \cos \gamma - \left( \frac{\sigma B_0^2(x)}{\rho} + \frac{\mu}{\rho k} \right) u, \quad (2)$$

$$u \frac{\partial N^*}{\partial x} + v \frac{\partial N^*}{\partial y} = \left( \frac{\gamma^*}{j^* \delta} \right) \frac{\partial^2 N^*}{\partial y^2} - \left( \frac{K_1^*}{j^* \delta} \right) \left( 2N^* + \frac{\partial u}{\partial y} \right), \quad (3)$$

$$u \frac{\partial T}{\partial x} + v \frac{\partial T}{\partial y} = \alpha \frac{\partial^2 T}{\partial y^2} + \tau \left[ D_B \frac{\partial C}{\partial y} \frac{\partial T}{\partial y} + \frac{D_T}{T_\infty} \left( \frac{\partial T}{\partial y} \right)^2 \right], \quad (4)$$

$$u \frac{\partial C}{\partial x} + v \frac{\partial C}{\partial y} = D_B \frac{\partial^2 C}{\partial y^2} + \frac{D_T}{T_\infty} \frac{\partial^2 T}{\partial y^2}, \quad (5)$$

Where in the directions  $x$  and  $y$  the velocity constituents are  $u$  and  $v$ , individually,  $g$  is the gravitational acceleration, the uniform magnetic field strength is given by  $B_0$ ,  $\sigma$  denotes the electrical conductivity, the viscosity is denoted by  $\mu$ , the density of the base liquid is given by  $\delta_f$ , the density of the nanoparticle is given by  $\delta_p$ , the vortex viscosity is defined as  $k_1^*$ , factor of thermal increase is given by  $\beta_t$ ,  $\beta_c$  denotes constant of concentration extension, the gyration ascent viscosity is given by  $\gamma^*$ , the micro inertia each component mass is given by  $j^*$ , the micro-rotation is given by  $N^*$ ,  $D_B$  denote the Brownian dispersal factor and  $D_T$  denotes the thermophoresis dispersion amount,  $k$  is the thermal conductivity, the heat capacity of the nanoparticles is denoted by  $(\delta c)_p$ ,  $(\delta c)_f$  represents the heat capacity of the conventional liquid, thermal diffusivity parameter is denoted by  $\alpha = \frac{k}{(\delta c)_f}$  and the relation among the active heat capacity of the nanoparticle and heat capacity of the liquid is represented by  $\tau = \frac{(\delta c)_p}{(\delta c)_f}$ .

The subject boundary conditions are

$$\begin{aligned} u &= u_w(x) = ax, v = 0, T = T_w, N^* = -m_0 \frac{\partial u}{\partial y}, C = C_w \quad \text{at } y = 0, \\ u &\rightarrow u_\infty(x) = 0, v \rightarrow 0, T \rightarrow T_\infty, N^* \rightarrow 0, C \rightarrow C_\infty \quad \text{at } y \rightarrow \infty, \end{aligned} \quad (6)$$

The nonlinear ordinary differential equations are obtained from nonlinear partial differential equations. The stream function  $\psi = \psi(x, y)$  use for this procedure is given as

$$u = \frac{\partial \psi}{\partial y}, \quad v = -\frac{\partial \psi}{\partial x}, \quad (7)$$

Where, equation (1) i.e. continuity equation is fulfilled identically. The similarity transformations are characterized as

$$u = axf'(\eta), v = -\sqrt{av}f(\eta), \eta = y\sqrt{\frac{a}{v}}$$

$$\theta(\eta) = \frac{T-T_\infty}{T_w-T_\infty}, \phi(\eta) = \frac{C-C_\infty}{C_w-C_\infty}, \quad (8)$$

On substituting equation (8), system of equations (2) to (5) converted to the following nonlinear ordinary differential equations:

$$(1+k)f''' + ff'' - f'^2 + kh' + (\lambda g + \delta q)\cos\gamma - (M + K_1)f' = 0, \quad (9)$$

$$\left(1 + \frac{k}{2}\right)h'' + fh' - f'h - k(2h + f'') = 0, \quad (10)$$

$$\left(\frac{1}{Pr}\right)\theta'' + f\theta' + Nb\phi'\theta' + Nt\theta'^2 = 0, \quad (11)$$

$$\phi'' + Le f\phi' + Nt_b\theta'' = 0, \quad (12)$$

Where

$$\lambda = \frac{Gr_x}{Re_x}, \delta = \frac{Gc_x}{Re_x}, M = \frac{\sigma B_0^2(x)}{a\rho}, K_1 = \frac{\nu}{ak}, Le = \frac{\nu}{D_B}, Pr = \frac{\nu}{\alpha}, Nb = \frac{\tau D_B(C_w - C_\infty)}{\nu}, Nt = \frac{\tau D_t(T_w - T_\infty)}{\nu T_\infty},$$

$$Nt_b = \frac{Nt}{Nb}, Gr_x = \frac{g\beta_t(T_w - T_\infty)x}{av}, Re_x = \frac{u_w(x)x}{\nu}, Gc_x = \frac{g\beta_c(C_w - C_\infty)x}{av}$$

$$(13)$$

Here, primes means the differentiation concerning  $\eta$ ,  $\lambda$  Buoyancy constraint, Solutal buoyancy parameter is given by  $\delta$ , the magnetic parameter is given by  $M$ , kinematic viscidness of the liquid is denoted by  $\nu$ ,  $Pr$  denotes the Prandtl number,  $Le$  denotes the Lewis number,  $K_1$  represents permeability factor,  $K$  is the dimensionless vertex thickness.

The corresponding boundary conditions are transformed to

$$f(\eta) = 0, f'(\eta) = 0, \theta(\eta) = 1, \phi(\eta) = 1 \text{ at } \eta = 0, \\ f'(\eta) \rightarrow 0, \theta(\eta) \rightarrow 0, \phi(\eta) \rightarrow 0 \text{ as } \eta \rightarrow \infty, \quad (14)$$

The skin friction, Sherwood number and Nusselt number for the present problem are defined as

$$Nu_x = \frac{xq_w}{k(T_w - T_\infty)}, Sh_x = \frac{xq_m}{D_B(C_w - C_\infty)}, C_f = \frac{\tau_w}{u_w^2 \rho_f} \quad (15)$$

The related terms for the skin-friction factor  $C_{fx}(0) = f''(0)$ , the reduced Nusselt number  $-\theta'(0)$  and the reduced Sherwood number  $-\phi'(0)$  are defined as

$$-\theta'(0) = \frac{Nu_x}{\sqrt{Re_x}}, -\phi'(0) = \frac{Sh_x}{\sqrt{Re_x}}, C_{fx} = C_f \sqrt{Re_x} \quad (16)$$

Where,  $Re_x = \frac{u_w(x)x}{\nu}$ , is the local Reynolds number built on the extending velocity. The converted nonlinear differential equations (9) to (12) by applying equation (14) are elucidated by

Keller box scheme consisting on the steps as, finite-differences technique, Newton's scheme and block elimination process clearly explained by Anwar et al. [30].

### 3 Results and Discussion

This portion of study deals with the calculated results of converted nonlinear ordinary differential equations (9-12) with boundary conditions (14) solved via Keller-box method. For numerical result of physical parameters of our concern including Brownian motion constraint  $Nb$ , thermophoresis constraint  $Nt$ , magnetic factor  $M$ , buoyancy factor  $\lambda$ , solutal buoyancy factor  $\delta$ , inclination factor  $\gamma$ , Prandtl number  $Pr$ , Lewis number  $Le$ , and material factor  $K$  several figures and tables are prepared. In Table 3.1, in the deficiency of buoyancy factor  $\lambda$ , solutal buoyancy factor  $\delta$ , magnetic factor  $M$ , porosity parameter  $K_1$  and material parameter  $K$  with  $\gamma = 90^\circ$  outcomes for reduced Nusselt number  $-\theta'(0)$ , reduced Sherwood number  $-\phi'(0)$  are equated with the existing results of Khan and Pop [31]. The consequences are established brilliant settlement. The effects of reduced Nusselt number  $-\theta'(0)$ , reduced Sherwood number  $-\phi'(0)$  and skin friction coefficient  $C_{fx}(0)$  against altered values of involved physical parameters  $Nb, Nt, M, K, \lambda, \delta, \gamma, K_1, Le$ , and  $Pr$  are shown in table 3.2. It is eminent that  $-\theta'(0)$  declines for increasing the values of  $Nb, Nt, M, Le, K_1, \gamma$ , and increased by enhancing the numerical values of  $K, \lambda, \delta$ , and  $Pr$ . Moreover, it is perceived that  $-\phi'(0)$  enhanced with the larger values of  $Nb, \lambda, \delta, Nt, Le, K$  and drops for bigger values of  $M, K_1, Pr$  and  $\gamma$ . On the other hand,  $C_{fx}(0)$  rises with the growing values of  $Nb, Le, M, K, \gamma, K_1$ , and drops with the higher values of  $Nt, \lambda, \delta$ , and  $Pr$ .

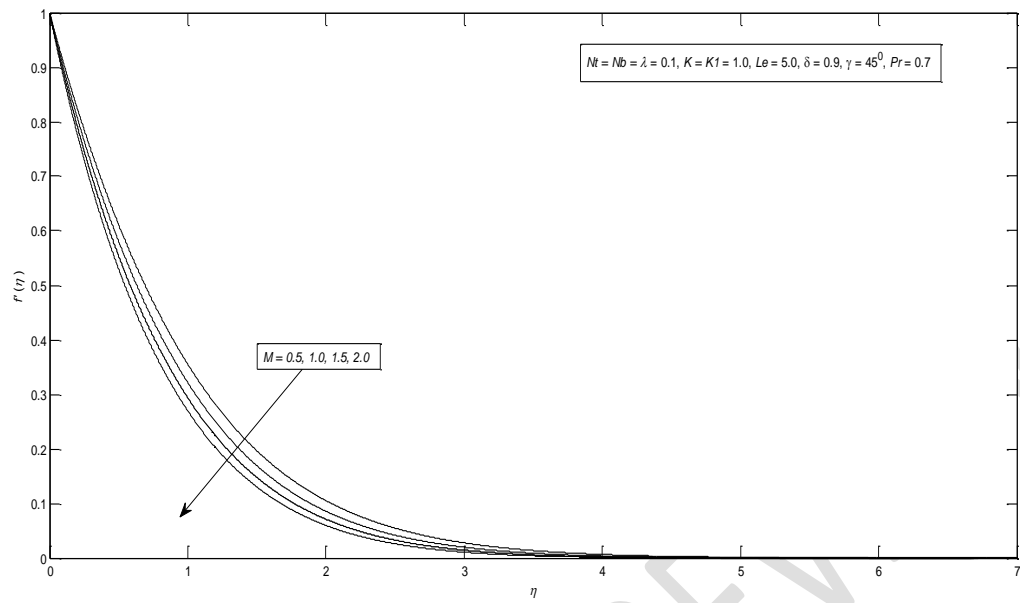
**Table 3.1:** Contrast of the reduced Nusselt number  $-\theta'(0)$  and the reduced Sherwood number  $-\phi'(0)$  when  $M, K, K_1, \delta, \lambda = 0$ ,  $Pr = Le = 10$  and  $\gamma = 90^\circ$ .

$Nb$	$Nt$	Khan and Pop (2010)		Present Results	
		$-\theta'(0)$	$-\phi'(0)$	$-\theta'(0)$	$-\phi'(0)$
0.1	0.1	0.9524	2.1294	0.9524	2.1294
0.2	0.2	0.3654	2.5152	0.3654	2.5152
0.3	0.3	0.1355	2.6088	0.1355	2.6088
0.4	0.4	0.0495	2.6038	0.0495	2.6038
0.5	0.5	0.0179	2.5731	0.0179	2.5731

205 **Table 3.2:** Values of the reduced Nusselt number  $-\theta'(0)$ , the reduced Sherwood number  
206  $-\phi'(0)$  and the Skin-friction coefficient  $C_{fx}(0)$ .

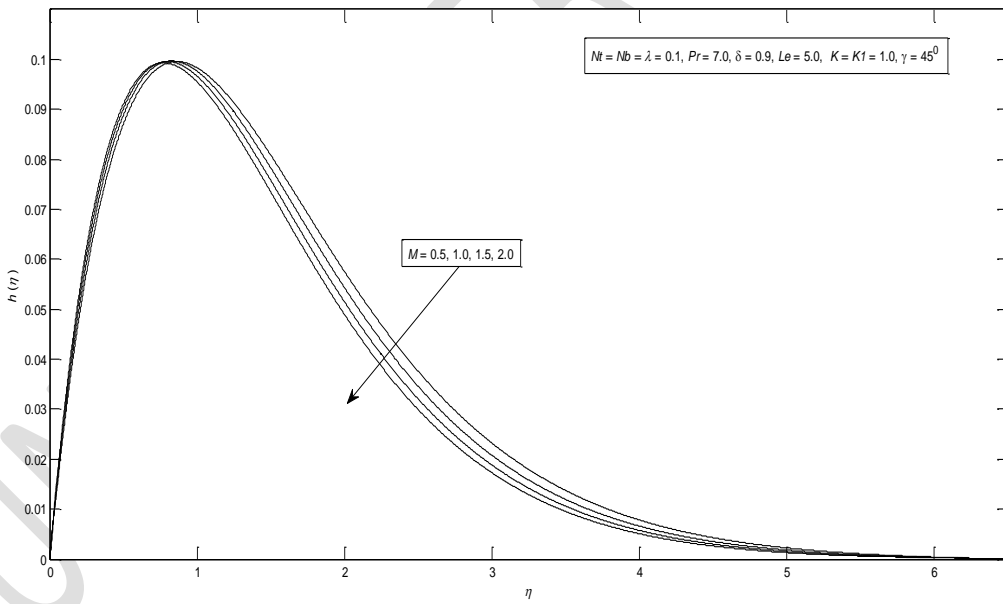
$Nb$	$Nt$	$Pr$	$Le$	$M$	$K$	$\lambda$	$\delta$	$KI$	$\gamma$	$-\theta'(0)$	$-\phi'(0)$	$C_{fx}(0)$
0.1	0.1	7.0	5.0	0.5	1.0	0.1	0.9	1.0	$45^0$	1.1054	1.0880	1.8913
<b>0.5</b>	0.1	7.0	5.0	0.5	1.0	0.1	0.9	1.0	$45^0$	0.2060	1.6011	1.9459
0.1	<b>0.5</b>	7.0	5.0	0.5	1.0	0.1	0.9	1.0	$45^0$	0.5104	1.3906	1.7176
0.1	0.1	<b>10.0</b>	5.0	0.5	1.0	0.1	0.9	1.0	$45^0$	1.1531	1.0852	1.8882
0.1	0.1	7.0	<b>10.0</b>	0.5	1.0	0.1	0.9	1.0	$45^0$	0.9672	2.0567	1.9689
0.1	0.1	7.0	5.0	<b>1.0</b>	1.0	0.1	0.9	1.0	$45^0$	1.0949	1.0550	2.1075
0.1	0.1	7.0	5.0	0.5	<b>3.0</b>	0.1	0.9	1.0	$45^0$	1.1331	1.1755	2.6215
0.1	0.1	7.0	5.0	0.5	1.0	<b>0.5</b>	0.9	1.0	$45^0$	1.1090	1.0963	1.8040
0.1	0.1	7.0	5.0	0.5	1.0	0.1	<b>2.0</b>	1.0	$45^0$	1.1195	1.1254	1.5847
0.1	0.1	7.0	5.0	0.5	1.0	0.1	0.9	<b>2.0</b>	$45^0$	1.0851	1.0246	2.3071
0.1	0.1	7.0	5.0	0.5	1.0	0.1	0.9	1.0	<b><math>90^0</math></b>	1.0917	1.0507	2.1758





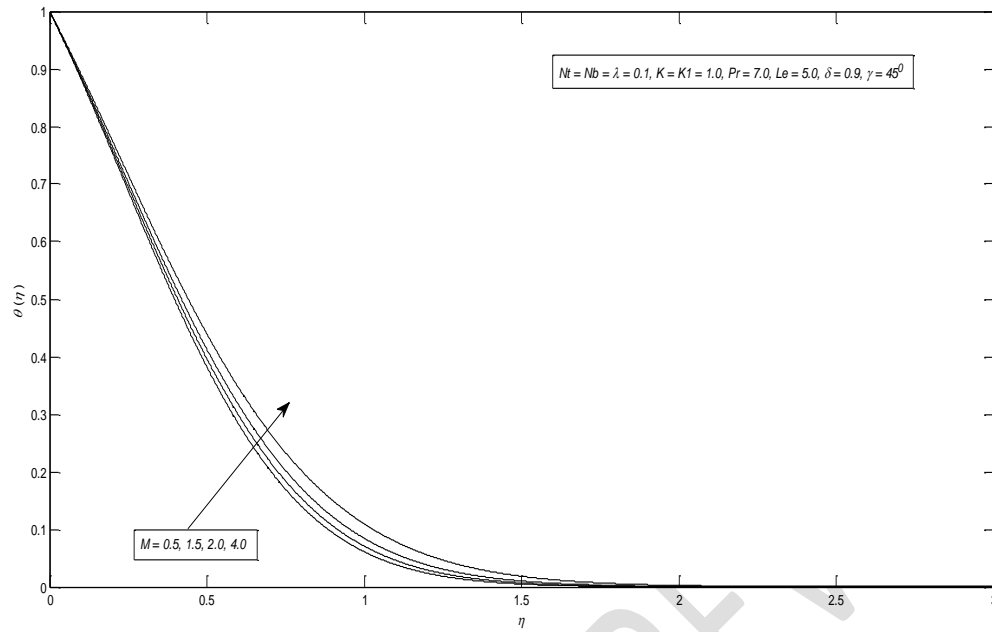
208

209 Fig. 2. Variations in velocity profile for several values of  $M$ .



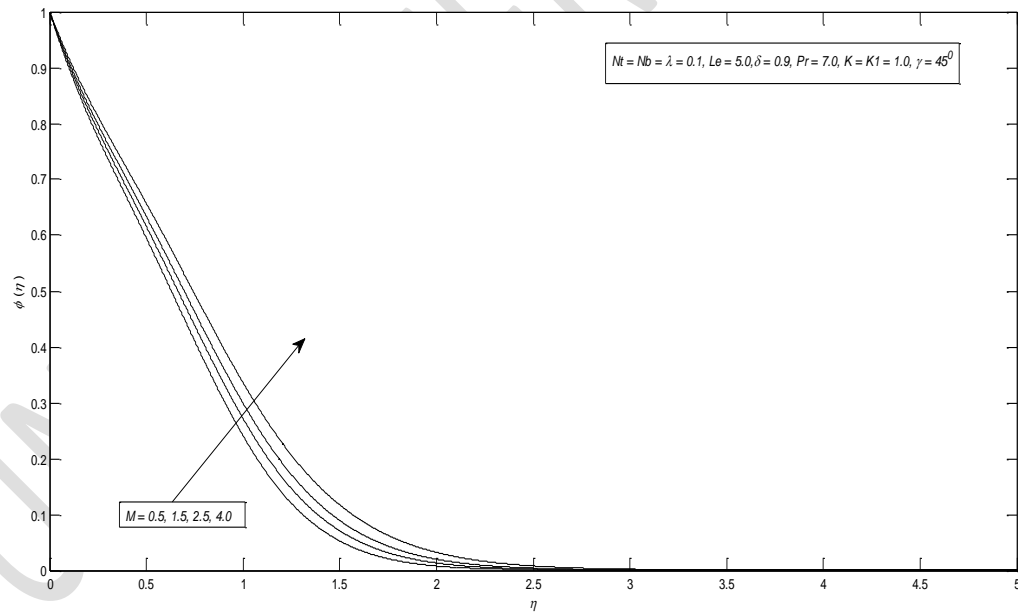
210

211 Fig. 3. Variations in angular velocity for several values of  $M$ .



212

213 Fig. 4. Variations in temperature profile for several values of  $M$ .

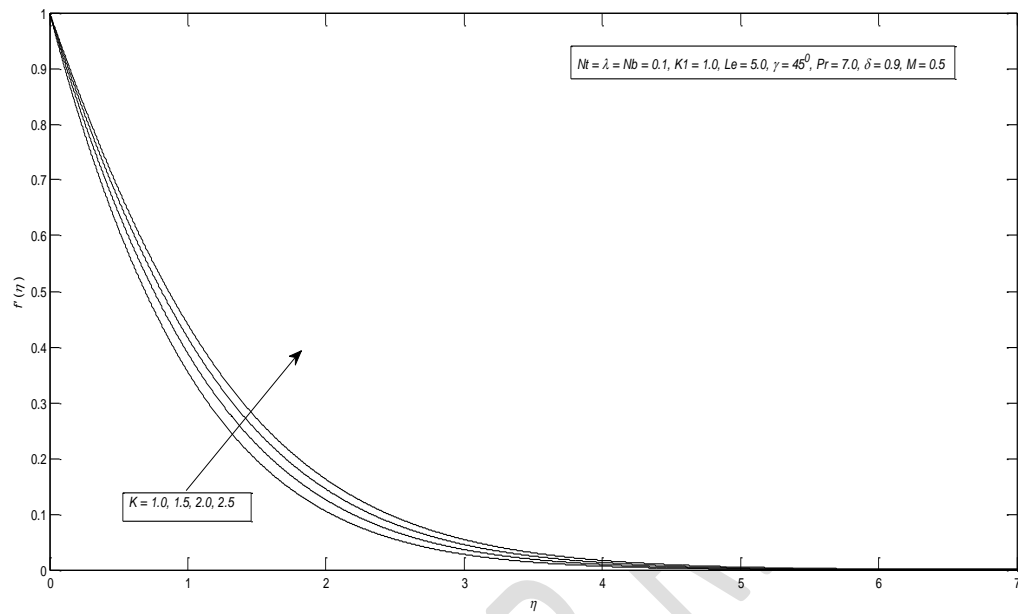


214

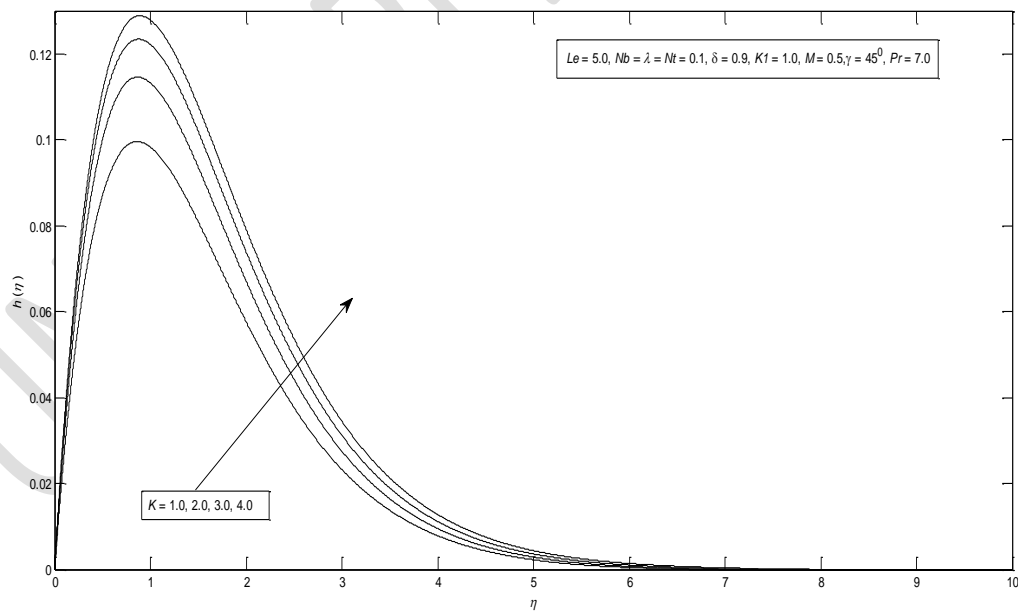
215 Fig. 5. Variations in concentration profile for several values of  $M$ .

216 Fig. 2 gives a picture of the upshot of factor  $M$  on velocity profile. The velocity outline slow  
 217 down as we upsurge the magnetic field constraint  $M$ . It is since the use of magnetic field yields  
 218 Lorentz force, by means retard the speed of the fluid. The similar result has seen in the instance

219 of the angular velocity against changed values of  $M$  in Fig. 3. Whereas, the different impacts of  
 220  $M$  on the temperature distribution presented in Fig. 4 and concentration profile in Fig. 5.



221  
 222 Fig. 6. Variations in velocity profile for several values of  $K$ .



223  
 224 Fig. 7. Variations in angular velocity profile for several values of  $K$ .

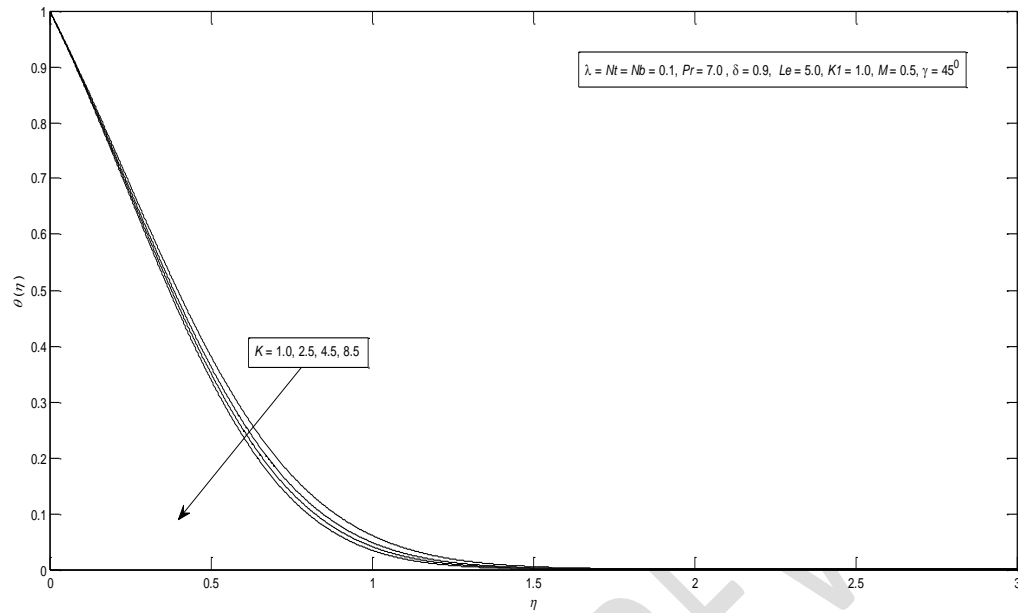


Fig. 8. Variations in temperature profile for several values of  $K$ .

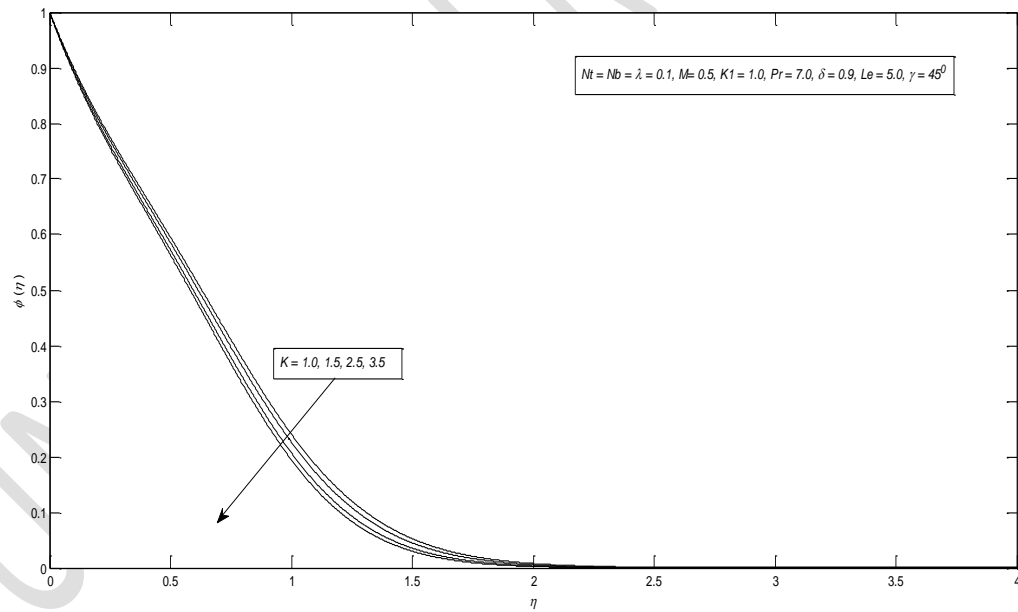


Fig. 9. Variations in concentration profile for several values of  $K$ .

It is noticed in Fig.6 the velocity profile upturn by enhancing the values of  $K$ . The angular velocity profile rise by growing the values of  $K$  indicates in Fig. 7. The boundary layer thickness

losses by improving the values of  $K$ . On the other hand Figs. 8 and 9 depict the opposite effects against different values of  $K$ .

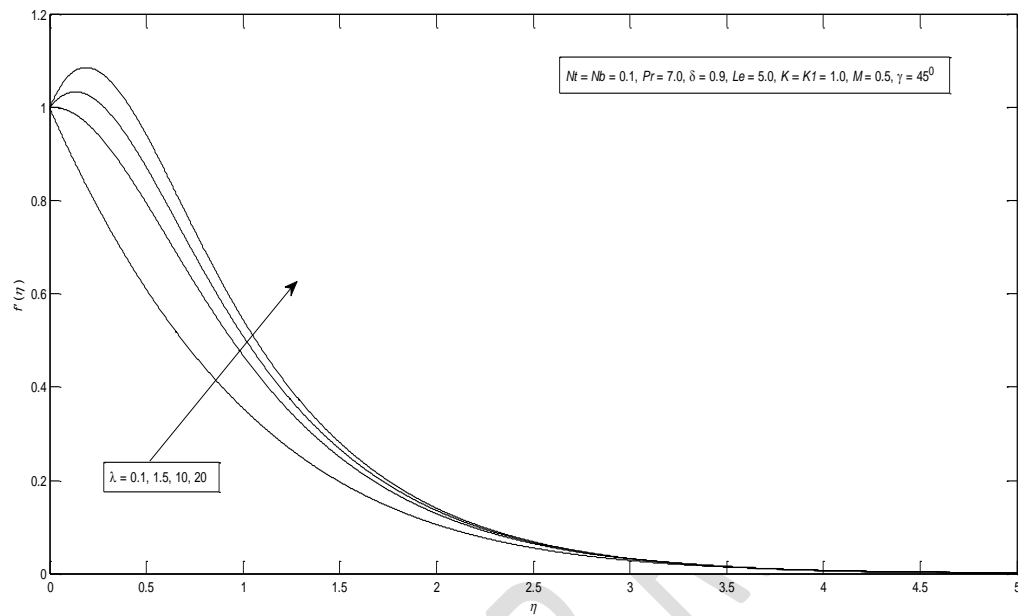


Fig. 10. Variations in velocity profile for several values of  $\lambda$ .

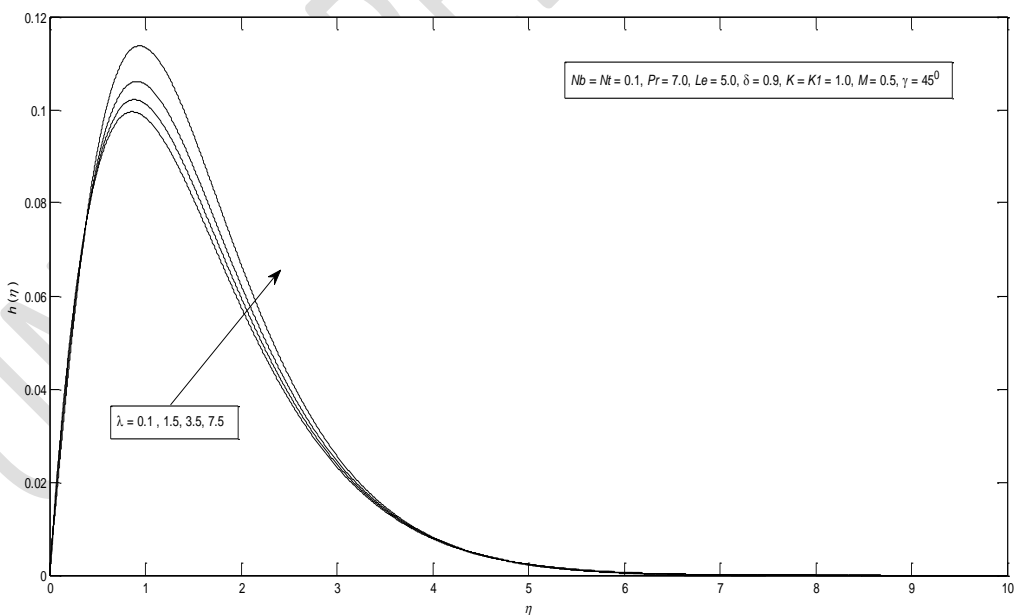
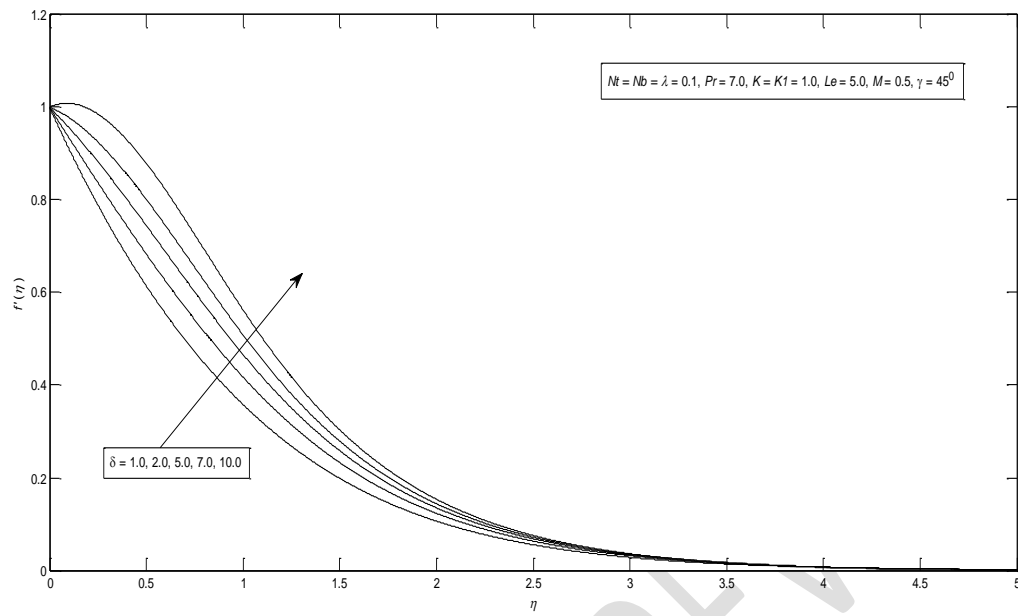
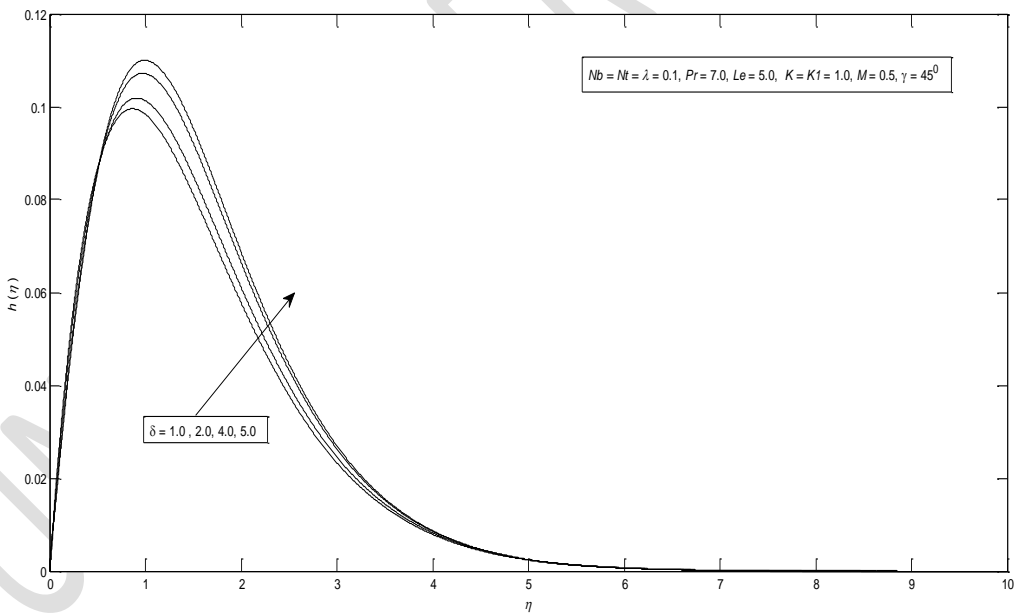


Fig. 11. Variation in angular velocity profile for several values of  $\lambda$ .



237

238 Fig. 12. Variations in velocity profile for several values of  $\delta$ .

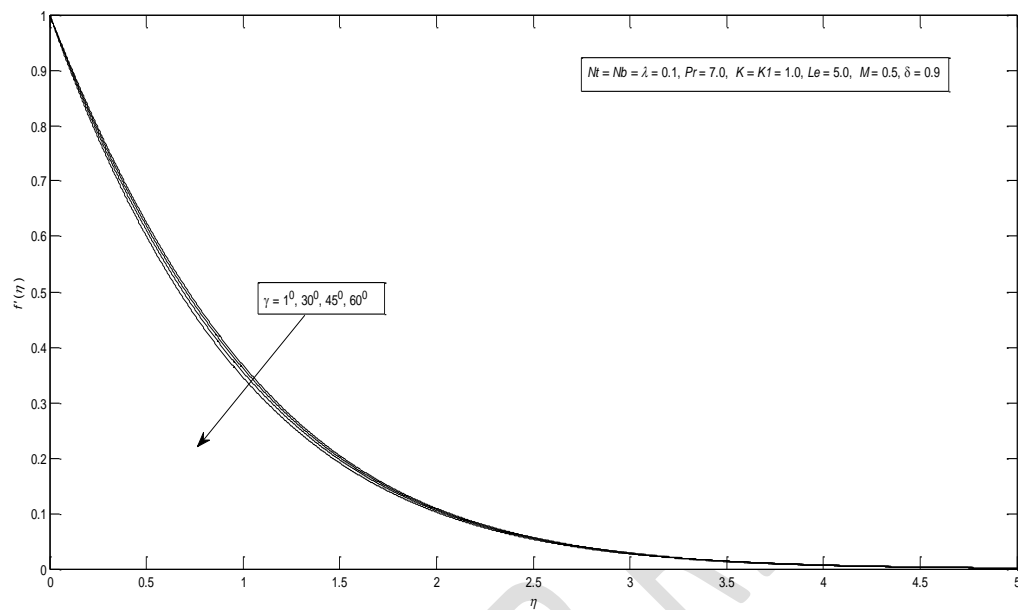


239

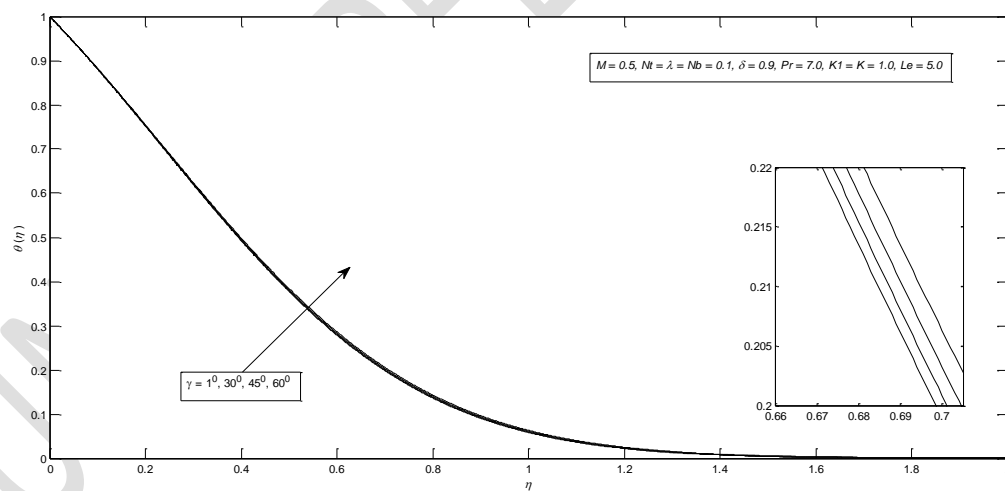
240 Fig. 13. Variations in angular velocity profile for several values of  $\delta$ .

241 The velocity shape upturns in Fig. 10 by enhancing bouncy parameter  $\lambda$ . Similarly the angular  
 242 velocity also enhanced with large values of  $\lambda$  clearly shown in Fig. 11. Moreover, the similar

243 result for solutal bouncky parameter  $\delta$  on velocity distribution and angular velocity contour  
 244 prominent in Figs.12 and 13.



245  
 246 Fig. 14. Variations in velocity profile for several value of  $\gamma$ .



247  
 248 Fig. 15. Variations in temperature profile for several values of  $\gamma$ .

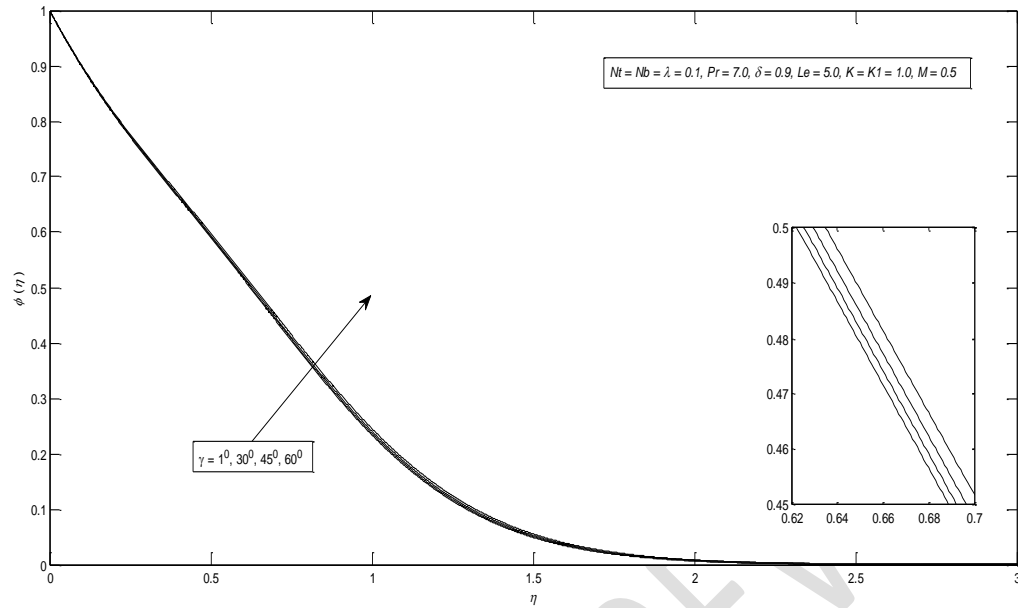


Fig. 16. Variations in concentration profile for several values of  $\gamma$ .

Fig. 14 portrays the consequence of inclination factor  $\gamma$  on velocity outline. It is openly perceived the velocity outline depreciate as we enhance the values of inclination parameter  $\gamma$ . This can be ascribed to the circumstance that the maximum gravitational force act on flow when the inclination parameter  $\gamma = 0$  because in this situation the sheet will be vertical. On the other hand, for  $\gamma = 90^0$  the sheet will be horizontal which cause the reduction in the velocity profile as the strength of the bouncy forces decrease. Besides, opposite result recovered in Figs. 15 and 16 for large values of inclination parameter  $\gamma$  in the instance of temperature and concentration sketches.



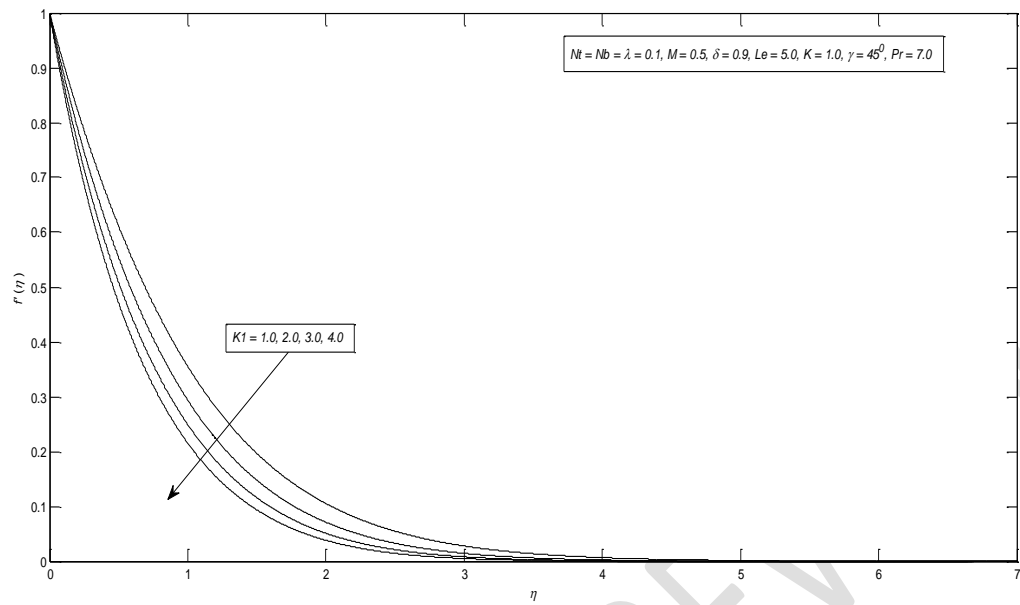


Fig. 17. Variations in velocity profile for several values of  $K_1$ .

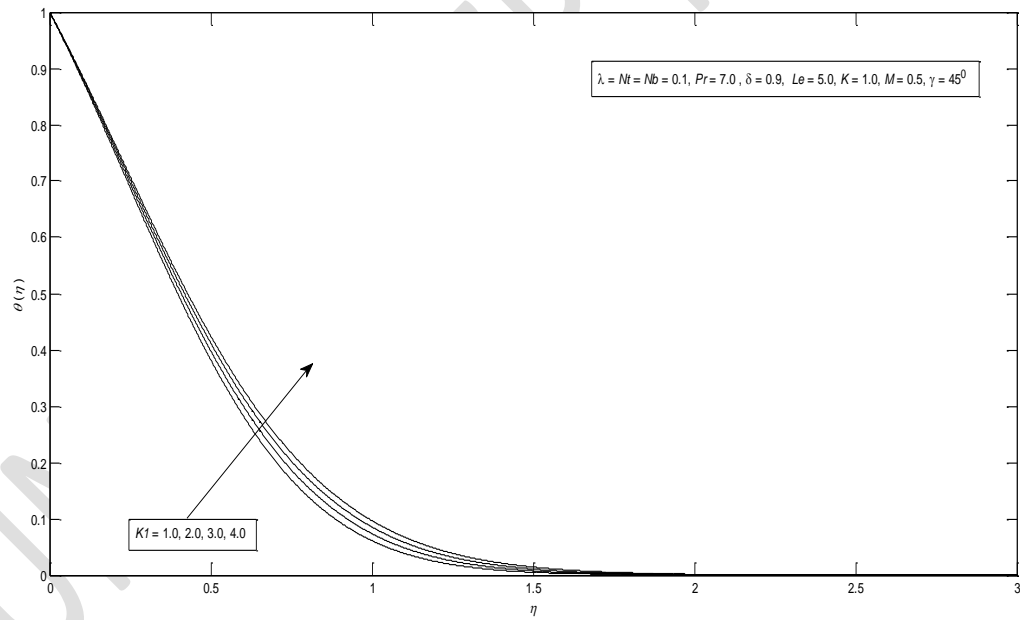


Fig. 18. Variations in temperature profile for several value of  $K_1$ .

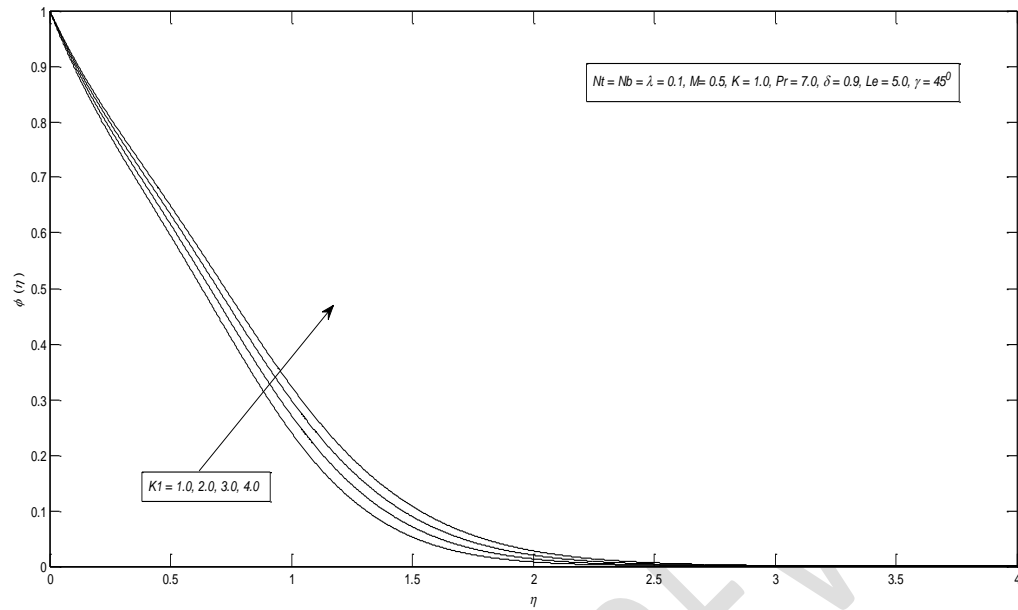


Fig. 19. Variations in concentration profile for several values of  $K_1$ .

It is well known that the porous medium offers high resistance that cause rising of shear stress. This shear stress work opposite to the fluid motion over a stretching sheet and fluid motion tends to slow. That's why, velocity profile illustrate reduction by increasing the values of  $K_1$  in this case as indicated by Fig. 17. Moreover, oppoite impact illustrate in Figs. 18 and 19 for verious values of  $K_1$ .

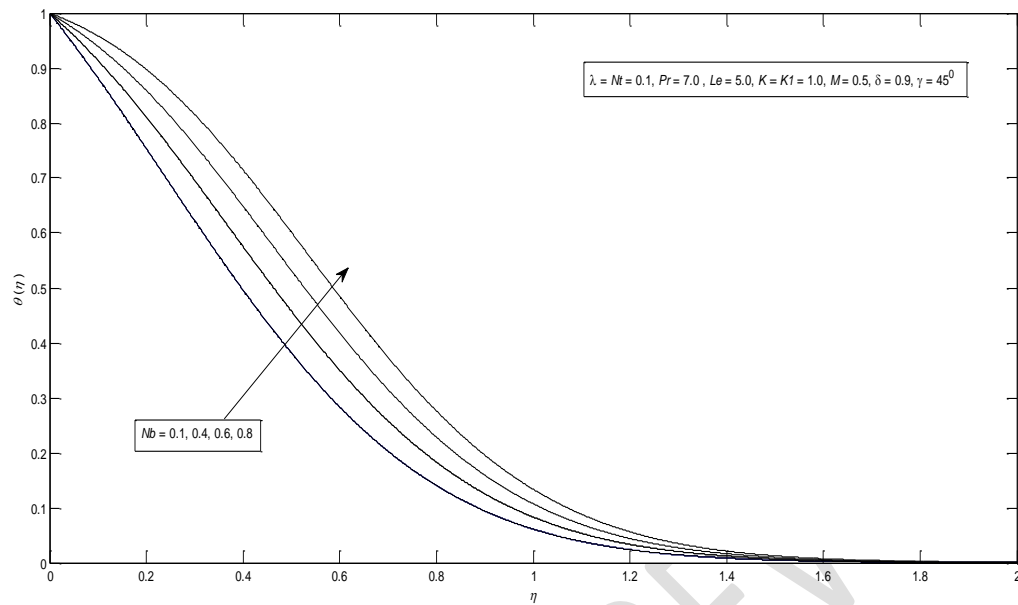


Fig. 20. Variations in temperature profile for several values of  $Nb$ .

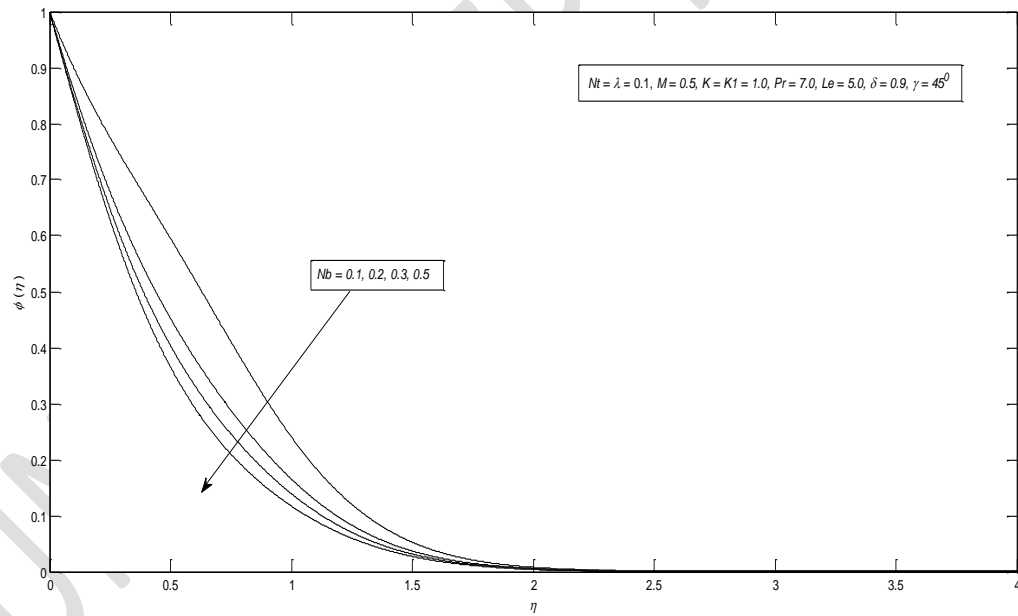
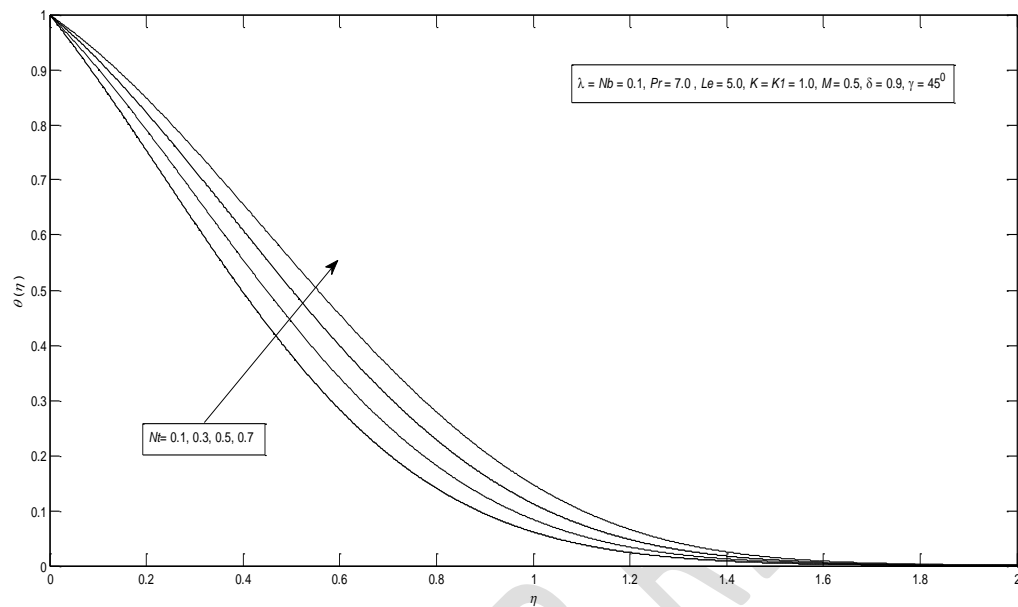


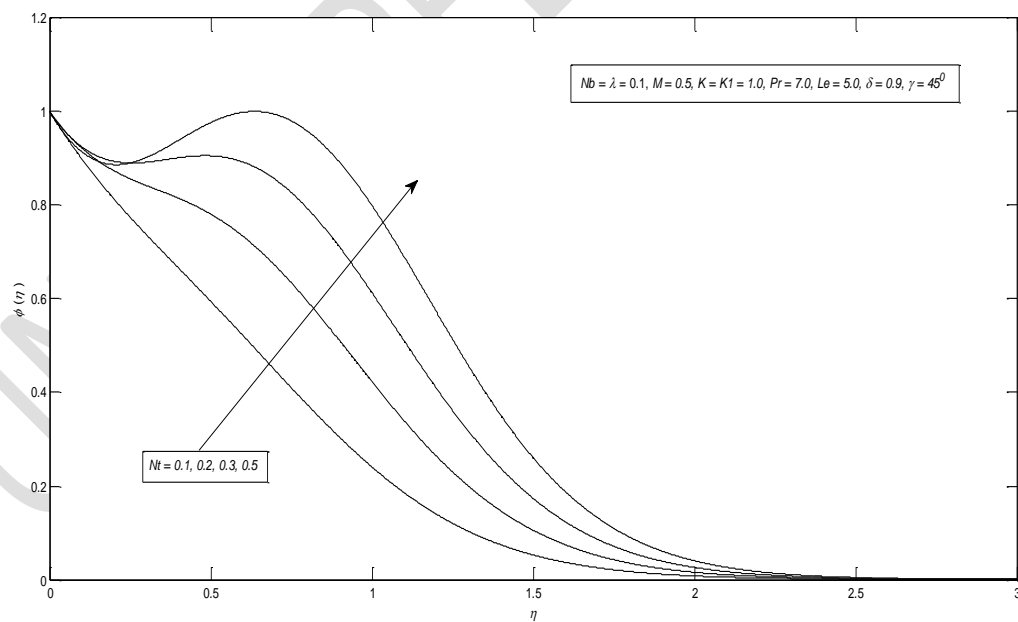
Fig. 21. Variations in concentration profile for several values of  $Nb$ .

Figures. 20 and 21 display the of effect of Brownian movement on the temperature and concentration sketches separately. The temperature sketch enlarges on enlarging  $Nb$ , on the other hand concentration distribution enlighten dissimilar style. Physically, boundary layer heat up due

277 to the development in Brownian motion which inclines to travel nanoparticles from the  
 278 extending sheet to the motionless liquid. Therefore the absorption nanoparticle lessens.



279  
 280 Fig. 22. Variations in temperature profile for several values of  $Nt$ .



281  
 282 Fig. 23. Variations in concentration profile for several values of  $Nt$ .

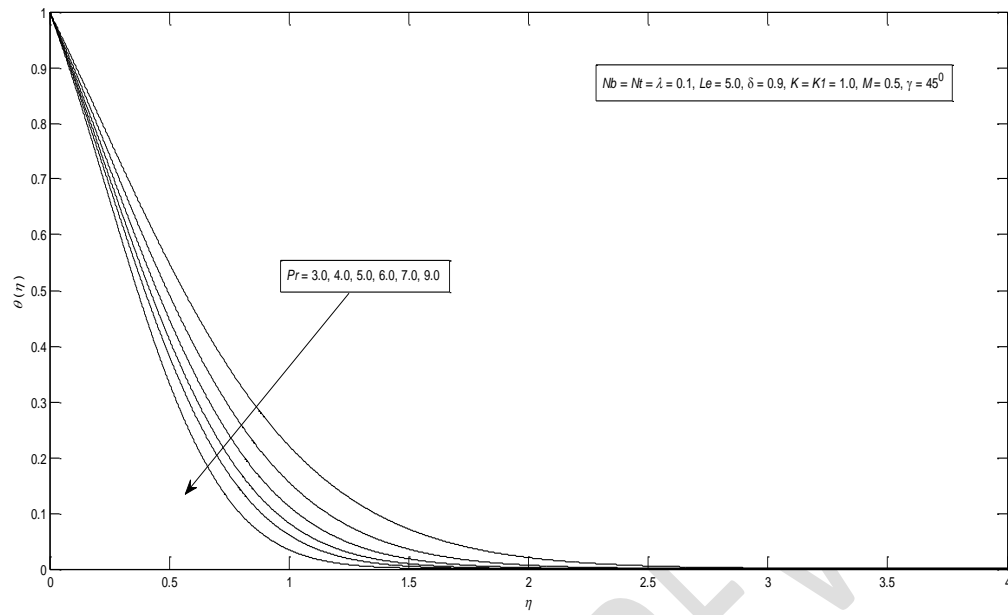


Fig. 24. Variations in temperature profile for several values of  $Pr$ .

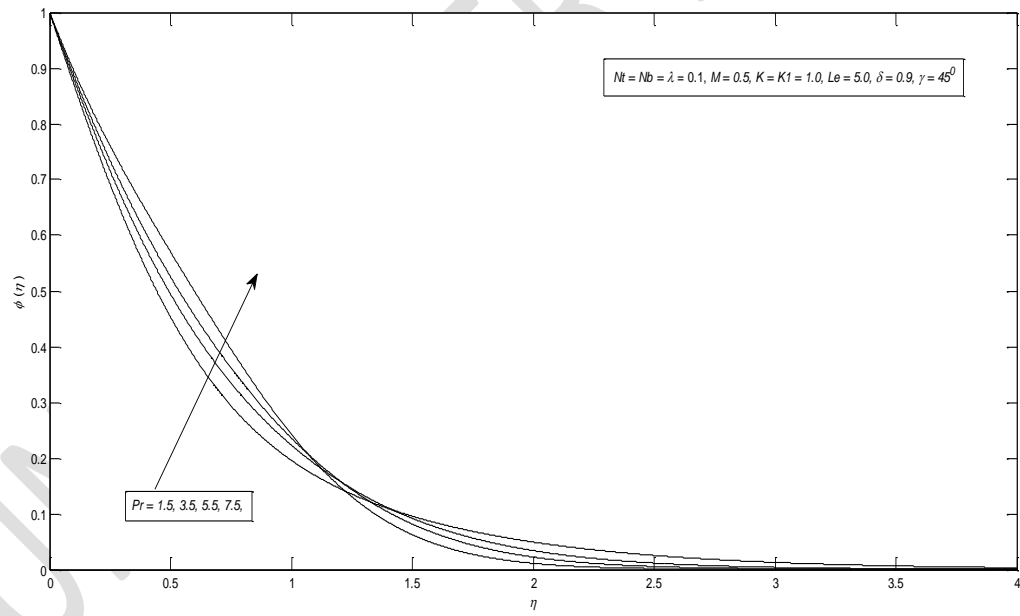


Fig. 25. Variations in concentration profile for several values of  $Pr$ .

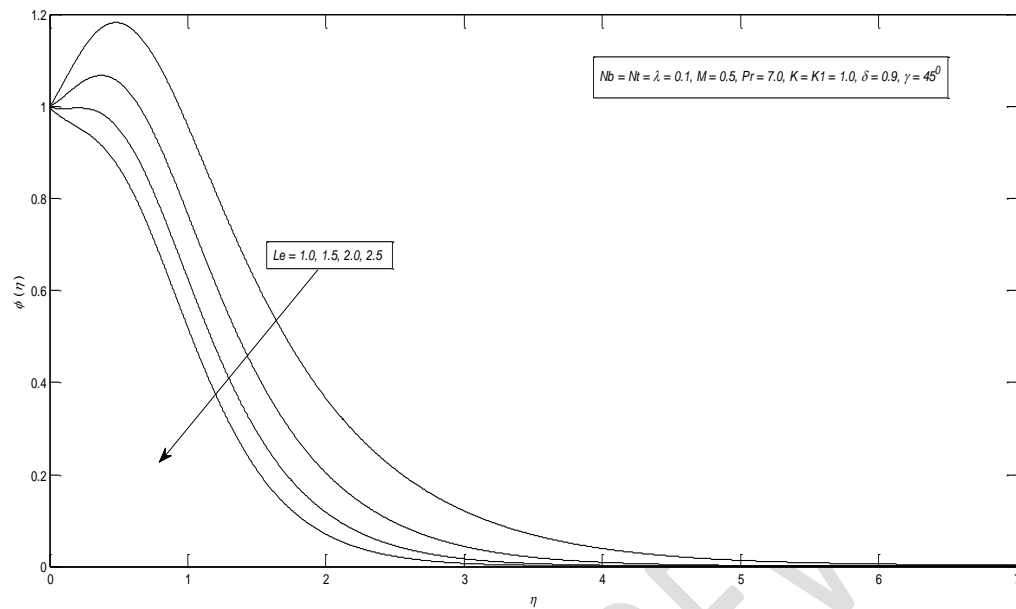


Fig. 26. Variations in concentration profile for several value of  $Le$ .

Figs. 22 and 23 present temperature and concentration profile against several values of thermophoresis parameters  $Nt$ . It is observed that both temperature and concentration contours upsurge by growing the thermophoresis parameter. Thermophoresis works to heat up boundary layer against several values of Prandtl number and Lewis number. Besides the amount of heat and mass exchange reduce by improving thermophoresis constraint  $Nt$ . Fig. 24 reveals that by growing the values of Prandtl number factor  $Pr$  the temperature profile drop, because thermal boundary layer viscosity declining by growing the Prandtl number  $Pr$ . In short an upturn in Prandtl number  $Pr$  mean deliberate amount of thermal dispersion. Whereas, concentration profile fall with large values of  $Pr$  presented in Fig. 25. Fig. 26 displays the result of Lewis number  $Le$  on concentration profile. The boundary layer viscosity lessening by improving the values of Lewis number  $Le$ .

#### 4 Conclusions

This study is explored the heat and mass exchange of micropolar nanofluid flow over linear inclined extending sheet. It is noted that  $-\theta'(0)$  falls for growing the values of  $Nb, Nt, M, Le, K_1, \gamma$ , and improved by enhancing the numerical values of  $K, \lambda, \delta$ , and  $Pr$ . Moreover, it is observed that  $-\phi'(0)$  boosted with the larger values of  $Nb, \lambda, \delta, Nt, Le, K$  and falls for bigger values of  $M, K_1, Pr$  and  $\gamma$ . On the other hand,  $C_{fx}(0)$  rises with the cumulative values of  $Nb, Le, M, K, \gamma, K_1$ , and falls with the higher values of  $Nt, \lambda, \delta$ , and  $Pr$ .

## References

- [1] Choi, S. U. S., Singer, D. A., & Wang, H. P. (1995). Developments and applications of non-Newtonian flows. *ASME FED*, 66, 99–105.
- [2] Buongiorno, J. (2006). Convective transport in nanofluids. *Journal of Heat Transfer*, 128(3), 240–250.
- [3] Zaimi, K., Ishak, A., & Pop, I. (2014). Boundary layer flow and heat transfer over a nonlinearly permeable stretching/shrinking sheet in a nanofluid. *Scientific Reports*, 4, 4404.
- [4] Anwar, M. I., Khan, I., Sharidan, S., & Salleh, M. Z. (2012). Conjugate effects of heat and mass transfer of nanofluids over a nonlinear stretching sheet. *International Journal of Physical Sciences*, 7(26), 4081–4092.
- [5] Sandeep, N., & Kumar, M. S. (2016). Heat and Mass Transfer in Nanofluid Flow over an Inclined Stretching Sheet with Volume Fraction of Dust and Nanoparticles. *Journal of Applied Fluid Mechanics*, 9(5).
- [6] Suriyakumar, P., & Devi, S. A. (2015). Effects of Suction and Internal Heat Generation on Hydromagnetic Mixed Convective Nanofluid Flow over an Inclined Stretching Plate. *European journal of advances in engineering and technology*, 2(3), 51–58.
- [7] Ziaei-Rad, M., Kasaeipoor, A., Rashidi, M. M., & Lorenzini, G. (2017). A Similarity Solution for Mixed-Convection Boundary Layer Nanofluid Flow on an Inclined Permeable Surface. *Journal of Thermal Science and Engineering Applications*, (c).  
<https://doi.org/10.1115/1.4035733>
- [8] Rashad, A. (2017). Unsteady nanofluid flow over an inclined stretching surface with convective boundary condition and anisotropic slip impact. *International Journal of Heat and Technology*, 35(1), 82–90. <https://doi.org/10.18280/ijht.350111>
- [9] Mitra, A. (2018). Computational Modelling of Boundary-Layer Flow of a Nano fluid Over a Convective Heated Inclined Plate. *JOURNAL OF MECHANICS OF CONTINUA AND MATHEMATICAL SCIENCES*, 13(2), 88–94.
- [10] Khan, M., Shahid, A., Malik, M. Y., & Salahuddin, T. (2018). Thermal and concentration diffusion in Jeffery nanofluid flow over an inclined stretching sheet: A generalized Fourier's and Fick's perspective. *Journal of Molecular Liquids*, 251, 7–14.
- [11] Hatami, M., Jing, D., & Yousif, M. A. (2018). Three-dimensional analysis of condensation nanofluid film on an inclined rotating disk by efficient analytical methods. *Arab Journal of Basic and Applied Sciences*, 25(1), 28–37.
- [12] Sakiadis, B. C. (1961). Boundary-layer behavior on continuous solid surfaces: I. Boundary-layer equations for two-dimensional and axisymmetric flow. *AIChE Journal*, 7(1), 26–28.

- [13] Crane, L. J. (1970). Flow past a stretching plate. *Zeitschrift Für Angewandte Mathematik Und Physik (ZAMP)*, 21(4), 645–647.
- [14] Ramesh, G. K., Gireesha, B. J., & Bagewadi, C. S. (2012). Heat transfer in MHD dusty boundary layer flow over an inclined stretching sheet with non-uniform heat source/sink. *Advances in Mathematical Physics*, 2012.
- [15] Singh, P. K. (2012). Heat and mass transfer in MHD boundary layer flow past an inclined plate with viscous dissipation in porous medium. *International Journal of Scientific & Engineering Research*, 3(6), 1–11.
- [16] Ali, M., Alim, M. A., & Alam, M. S. (2015). Similarity Solution of Heat and Mass Transfer Flow over an Inclined Stretching Sheet with Viscous Dissipation and Constant Heat Flux in Presence of Magnetic Field. *Procedia Engineering*, 105(Icte 2014), 557–569. <https://doi.org/10.1016/j.proeng.2015.05.089>
- [17] Ramesh, G. K., Chamkha, A. J., & Gireesha, B. J. (2015). Boundary layer flow past an inclined stationary/moving flat plate with convective boundary condition. *Afrika Matematika*. <https://doi.org/10.1007/s13370-015-0323-x>
- [18] Malik, M. Y., & Rehman, K. U. (2016). Effects of second order chemical reaction on MHD free convection dissipative fluid flow past an inclined porous surface by way of heat generation: A Lie group analysis. *Information Sciences Letters*, 5, 35–45.
- [19] Hayat, T., Qayyum, S., Alsaedi, A., & Asghar, S. (2017). Radiation effects on the mixed convection flow induced by an inclined stretching cylinder with non-uniform heat source/sink. *PloS one*, 12(4), e0175584.
- [20] Balla, C. S., Kishan, N., Gorla, R. S. R., & Gireesha, B. J. (2017). MHD boundary layer flow and heat transfer in an inclined porous square cavity filled with nanofluids. *Ain Shams Engineering Journal*, 8(2), 237–254.
- [21] Eringen, A. C. (1964). Simple microfluids. *International Journal of Engineering Science*, 2(2), 205–217.
- [22] Rahman, M. M., Aziz, A., & Al-Lawatia, M. A. (2010). Heat transfer in micropolar fluid along an inclined permeable plate with variable fluid properties. *International Journal of Thermal Sciences*, 49(6), 993–1002. <https://doi.org/10.1016/j.ijthermalsci.2010.01.002>
- [23] Das, K. (2012). Slip effects on heat and mass transfer in MHD micropolar fluid flow over an inclined plate with thermal radiation and chemical reaction. *International Journal for Numerical Methods in Fluids*, 70(1), 96–113.
- [24] Kasim, A. R. M., Mohammad, N. F., & Shafie, S. (2013). Unsteady MHD mixed convection flow of a micropolar fluid along an inclined stretching plate. *Heat Transfer—Asian Research*, 42(2), 89–99.
- [25] Srinivasacharya, D., & Bindu, K. H. (2016). Entropy generation in a micropolar fluid flow



through an inclined channel. *Alexandria Engineering Journal*, 55(2), 973–982.

[26] Hazbavi, A., & Sharhani, S. (2017). Micropolar Fluid Flow Between Two Inclined Parallel Plates. In *ASME 2017 International Mechanical Engineering Congress and Exposition* (p. V008T10A085-V008T10A085). American Society of Mechanical Engineers.

[27] Shamshuddin, M. D., Mishra, S. R., Bég, O. A., & Kadir, A. (2018). Unsteady reactive magnetic radiative micropolar flow, heat and mass transfer from an inclined plate with joule heating: A model for magnetic polymer processing. *Proceedings of the Institution of Mechanical Engineers, Part C: Journal of Mechanical Engineering Science*, 954406218768837.

[28] Srinivasacharya, D., RamReddy, C., & Naveen, P. (2018). Double dispersion effect on nonlinear convective flow over an inclined plate in a micropolar fluid saturated non-Darcy porous medium. *Engineering Science and Technology, an International Journal*.

[29] Mishra, S. R., Baag, S., & Mohapatra, D. K. (2016). Engineering Science and Technology , an International Journal Chemical reaction and Soret effects on hydromagnetic micropolar fluid along a stretching sheet. *Engineering Science and Technology, an International Journal*, 19(4), 1919–1928. <https://doi.org/10.1016/j.jestch.2016.07.016>

[30] Anwar, M. I., Shafie, S., Hayat, T., Shehzad, S. A., & Salleh, M. Z. (2017b). Numerical study for MHD stagnation-point flow of a micropolar nanofluid towards a stretching sheet. *Journal of the Brazilian Society of Mechanical Sciences and Engineering*, 39(1), 89–100. <https://doi.org/10.1007/s40430-016-0610-y>

[31] Khan, W. A., & Pop, I. (2010). Boundary-layer flow of a nanofluid past a stretching sheet. *International journal of heat and mass transfer*, 53(11-12), 2477-2483.